

Experimental and numerical study of microchannel formation in rubber-assisted hot embossing with an open-channel mold

Danyang Zhao¹ · Hairui Wang¹ · Longxian Wang¹ · Minjie Wang¹ · Donggang Yao²

Received: 9 November 2015 / Accepted: 1 March 2016 / Published online: 17 March 2016
© Springer-Verlag Berlin Heidelberg 2016

Abstract In comparison to conventional hot embossing with a precisely aligned pair of hard mold plates, the rubber-assisted hot embossing process with a modified embossing tool that employs only one hard mold plate containing through-thickness open microchannels was investigated both experimentally and numerically. The numerical process dynamics model was constructed using a hyperelastic constitutive model to describe the large deformation behavior of the embossing film at an embossing temperature near the glass transition temperature. Both experimental and numerical results showed that excellent replication of microchannel patterns can be achieved using the simplified tool setup and an embossing temperature slightly above T_g is suitable for achieving a uniform embossing thickness. Additional advantages from the use of open channels on the embossing mold include reduced diesel effect in the mold cavity and improved surface smoothness of the embossed film. The simulation results agreed very well with the experimental observations for the effects of the main process parameters on the replication quality, and this study demonstrated that the hyperelastic process model is capable of predicting the basic characteristics of the rubber-assisted embossing process with an open-channel embossing mold.

1 Introduction

In conventional hot embossing of shell-type microstructures, a matching pair of hard mold plates is used for defining the microstructures. In this case, precise alignment of the mating surfaces is required for successful feature transfer; a small misalignment may result in a mold failure or damage of the microstructures on the mold. By comparison, the rubber-assisted hot embossing process (Nagarajan and Yao 2006, 2009) employs one hard mold plate and one rubbery mold plate in place of a hard match pair so that precision alignment of mold plates is not necessary. The advantages of such a mold construction include simplification of the embossing tool, protection of the embossing master, buildup of uniform embossing pressure, and ease of demolding. Nagarajan and Yao (2011a, b) experimentally identified the effects of major process and material parameters, numerically studied the stress relaxation process, and predicted the elastic recovery in rubber-assisted hot embossing. The simulation results generally agree with the experimental observations when ABS was used as the embossing material, providing a quantitative insight into the deformation and stress relaxation processes.

Rubber-assisted hot embossing, to a large extent, is similar to conventional thermoforming and may be considered as a micro-thermoforming process. To further explore the advantages of such a micro-thermoforming process, Zhao et al. (2012) machined through-thickness microchannels on the hard mold plate and used them to define the shape of the micropattern. During embossing, the polymer film is forced into the open microchannels by the rubber pad, resembling a positive-pressure thermoforming process. This modified tooling not only simplifies the mold design but also produces smoother surfaces on the embossed film. Furthermore, air in the mold can be

✉ Danyang Zhao
zhaody@dlut.edu.cn

✉ Donggang Yao
yao@gatech.edu

¹ Dalian University of Technology, Dalian,
People's Republic of China

² Georgia Institute of Technology, Atlanta, GA, USA

freely displaced to avoid the unwanted diesel effect. The experimental study, however, also reveals the difficulty in conducting process optimization and achieving precision patterning; the thickness uniformity and depth of the embossed channel are significantly affected by various process conditions, including embossing temperature, embossing time, embossing pressure and rubber hardness (Zhao et al. 2012).

For thermoforming, computational modeling and simulation has evolved into a reliable and effective tool for process analysis and optimization (Worgull and Hecke 2004; Guo et al. 2007; Lan et al. 2009; Taylor et al. 2009; Srivastava et al. 2010; Park et al. 2011; Song et al. 2015). Particularly, hyperelastic models have been successfully used to model the deformation process in thermoforming and have achieved useful predications (Beda 2007; Nagarajan and Yao 2011b). For rubber-assisted embossing using a mold with through-thickness microchannels, Zhao et al. (2012) has shown that the rubbery plateau region is suitable for precision patterning. For embossing in this temperature range, the embossing film can also be considered hyperelastic. Therefore, it would be useful to establish a hyperelastic process model for guiding process design and optimization. However, due to the special process setting in rubber-assisted embossing, the standard modeling and simulation for thermoforming need to be modified to accommodate the new tooling setup and material selection, as well as the microgeometry. Additional issues need to be addressed that the replicated height of the microchannel is not simply controlled by the mold, but dictated by the rheological properties and the process conditions during rubber-assisted embossing.

In this work, a hyperelastic process model for rubber-assisted embossing was established. The process model was implemented using the finite element method and used to predict the deformation behavior of the embossing film under various processing conditions and compare with experimental results. The study focused on examining the feasibility of the hyperelastic process model for the rubber-assisted hot embossing process where a special mold with through-thickness microchannels is employed.

2 Modeling of process dynamics

Typically, the hot embossing process consists of five stages: preheating, embossing, holding, cooling and demolding. The polymer film after preheating undergoes large deformation in the isothermal embossing stage, which according to previous experimental results (Nagarajan and Yao 2011a; Zhao et al. 2012) is the main stage affecting the geometrical shape of the embossed film. The process dynamics model, therefore, is focused on the isothermal embossing stage.

2.1 Governing equations

During rubber-assisted hot embossing, the large-strain deformation of polymer near the glass transition temperature (T_g) cannot be easily modeled by molecular theory. The constitutive model for the hyperelastic material, instead, can be established using a continuum theory, which can be characterized by a strain energy density function (Beda 2007).

The common strain energy density function of an incompressible ($I_3 = 1$), homogenous and isotropic material can be written as a function of the invariants of the left Cauchy–Green deformation tensor

$$W = W(I_1, I_2) = \sum_{i=0, j=0}^{\infty} C_{ij}(I_1 - 3)^i(I_2 - 3)^j, \quad (1)$$

where I_1 and I_2 are the first and second invariants of the left Cauchy–Green deformation tensor.

A useful empirical model for the strain energy density function of a hyperelastic material is the two-parameter Mooney–Rivlin (M-R) model, written as

$$W = C_{10}(I_1 - 3) + C_{01}(I_2 - 3), \quad (2)$$

where C_{10} and C_{01} are the parameters of the M-R model, which can be obtained by fitting to experimental material properties.

For the uniaxial extension of a unit volume, the stress can then be expressed as

$$\begin{aligned} \sigma &= 2C_{10}\left(\lambda - \frac{1}{\lambda^2}\right) + 2C_{01}\left(1 - \frac{1}{\lambda^3}\right) \\ &= 2\left(C_{10} + \frac{C_{01}}{\lambda}\right)\left(\lambda - \frac{1}{\lambda^2}\right) \end{aligned} \quad (3)$$

where the invariants (I_1, I_2) of the Cauchy–Green deformation tensor are given by $I_1 = \lambda^2 + \frac{2}{\lambda}$ and $I_2 = \frac{1}{\lambda^2} + 2\lambda$ where λ is the principal elongational ratio or stretch.

The two parameters (C_{10}, C_{01}) of the M-R model are fitted by the stress–strain curve given by the uniaxial tension or compression test of the polymer. The embossing process can be modeled using a continuum mechanics approach with this hyperelastic material model. The resulting governing equations can then be solved using the finite element method (FEM). In this work, a commercial FEM code, ANSYS/Workbench, was used as a solver.

2.2 Geometrical model and boundary conditions

Several assumptions are made to simplify the analysis of the embossing process. Firstly, the length of the through-thickness microchannel is considered much larger than the width and the depth. Hence, the deformation is deemed to

be two-dimensional, and the polymer flow during cavity filling only depends on the width (x) and depth (z) directions of the polymer. Secondly, the effect of gravity is sufficiently small and can be neglected. Thirdly, it is assumed that the no-slip boundary condition applies at the contact between the polymer and the inner wall of the mold. The resulting two-dimensional plain strain model with a unit cavity of a microchannel is shown in Fig. 1. The arrows represent the flow directions of the rubber pad and the polymer film in the embossing stage.

Experimental studies of rubber-assisted embossing with silicone rubber (SR) and polystyrene (PS) film have previously been conducted by Zhao et al. (2012). The microchannels on the mold used in the experiments were 200 μm

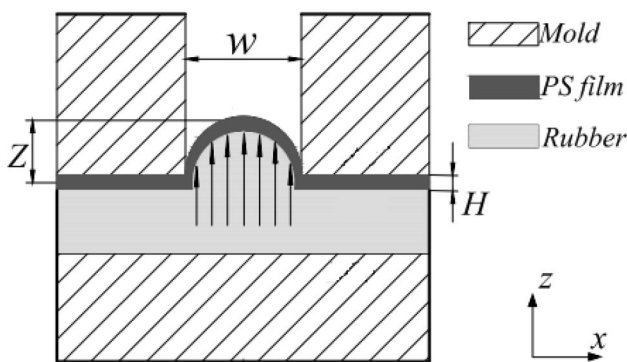


Fig. 1 Simplified model for rubber-assisted embossing with a through-thickness microchannel mold

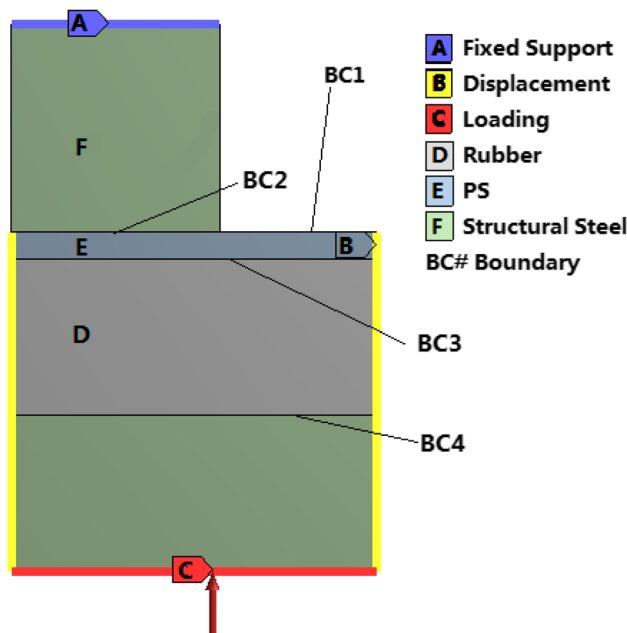


Fig. 2 The geometrical model

wide, and the PS film was 25 μm thick. The same dimensions are used in the simulation model for the microchannel width (w) and the polymer film thickness (H).

The geometrical model is shown in Fig. 2. Here, the boundaries are marked by BC#. The BC's are set up to approximate the physical contacts at each boundary. The upper surface of the PS film (i.e., BC2) is treated as a free surface with contact detection, and no wall slip occurs after contact. It is also proposed that the contact between the upper mold and the PS film (i.e., BC1) is a frictional contact, and the coefficient of friction is set to 0.1. The contact between the PS film and the SR pad (i.e., BC3) and the contact between the SR pad and the lower mold (i.e., BC4) are both considered as a bonded material interface. Fixed displacement is applied to the upper surface of the upper mold (A). The geometrical model is considered periodic, and zero x displacement is applied to the side face (B). During the embossing process, a load is applied to the lower surface of the mold (C). Due to the symmetry of the geometry and boundary conditions, only half of the geometry was actually used in the simulation.

The model described above was numerically solved by the finite element method using ANSYS. The embossing simulation was performed under varied embossing temperature ranging from 90 to 110 $^{\circ}\text{C}$, varied embossing load from 7.5 to 17.5 kN, and varied Shore hardness of SR sheets from 30 to 60 A.

2.3 Material properties

The mold made of steel is considered relatively rigid, and its deformation is rather small as compared with that of the polymer. During embossing, the PS film is deformed at

Table 1 Material parameters used in the simulation

Material	PS	SR	Mold
Young's modulus (GPa)	–	–	210
Poisson's ratio	0.330	–	0.250
Density (Kg/m ³)	1050	1100	7810



Fig. 3 Geometry of SR samples for uniaxial tensile testing

temperature above the glass transition temperature, and the silicone rubber pad serves as a soft counter-tool for squeezing the PS film between the rubber pad and the steel mold. In such a deformation process, the mold can be considered as a linear elastic material, but the deformation of the PS film and the rubber pad is large and nonlinear. Table 1 lists the properties of these materials. The elastic properties of the two hyperelastic materials, PS and SR, were determined experimentally as elaborated as follows.

Silicone rubber contains numerous silicon–oxygen bonds with high bonding energy. Its mechanical properties, in general, are stable and consistent between -60 °C and 250 °C. Experimental stress–strain curves were obtained from dog-bone samples of SR sheets, as shown in Fig. 3. The uniaxial tensile test was performed at room temperature on a universal testing machine (CMT4204, MTS USA) following ASTM D 412.

Figure 4 shows tensile stress–strain curves of SR sheets with varied Shore hardness. The fitted stress–strain curves from the M-R model in accordance with Eq. (3) are also included in the same figure. The corresponding fitting parameters are summarized in Table 2.

The stress–strain curves of the PS film under different temperature have been previously reported (Zhao et al. 2012). The fitted stress–strain curves from the M-R model in accordance with Eq. (3) are included in Fig. 5. An obvious nonlinearity can be seen at the testing temperature 110 °C.

The corresponding fitting parameters are summarized in Table 3. The PS film was modeled as a linear elastic

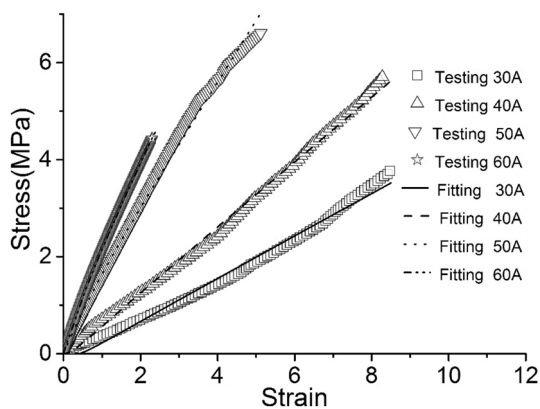


Fig. 4 Comparison of SR stress–strain curves between experimental and fitting data

Table 2 M-R fitting parameters of SR with different hardness

Fitting parameter	30 A	40 A	50 A	60 A
C_{10}	0.218	0.334	0.628	0.814
C_{01}	-0.309	-0.355	-0.321	-0.403

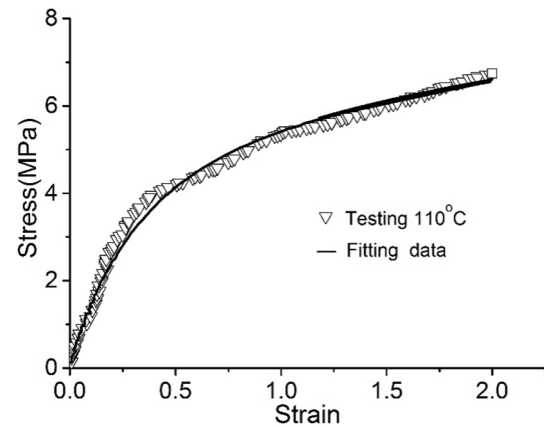


Fig. 5 Comparison of PS stress–strain curves between experimental and fitting data

Table 3 M-R fitting parameters of PS with different temperature

Parameter (MPa)	90 °C	100 °C	110 °C
Young's modulus	439	158	–
C_{10}	–	–	0.321
C_{01}	–	–	2.467

material at 90 and 100 °C. At 110 °C, a two-parameter M-R model was used to model the constitutive behavior of PS.

3 Experimental embossing

Rubber-assisted embossing experiments were conducted using a steel mold with a through-thickness microchannel, as shown in Fig. 6. The microchannel was made using wire EDM (electrical discharge machining). Three through-thickness wells are also included; after embossing, these wells become pockets on the embossed film which can serve as fluid pockets for fluidic transport.

Biaxially oriented PS film with a thickness of 25 μm was used in the embossing experiments (Catalog number LS378801 MKS obtained from Goodfellow Corporation). The same type of PS film was also used in the previous work (Zhao et al. 2012), and it demonstrated good replication quality in rubber-assisted embossing. The T_g of the PS film is known to be 100 °C. SR sheets were obtained from Shenzhen Yizhong Rubber Corporation. The thickness and Shore hardness are 8 mm and 30–60 A, respectively. Several pads of 70 mm diameter were cut out from these SR sheets and used as soft counter-tools.

A compression molding machine equipped with lower and upper platens supplied by Shenzhen Chuangjiahong Machinery Co. Ltd was used as an apparatus for hot

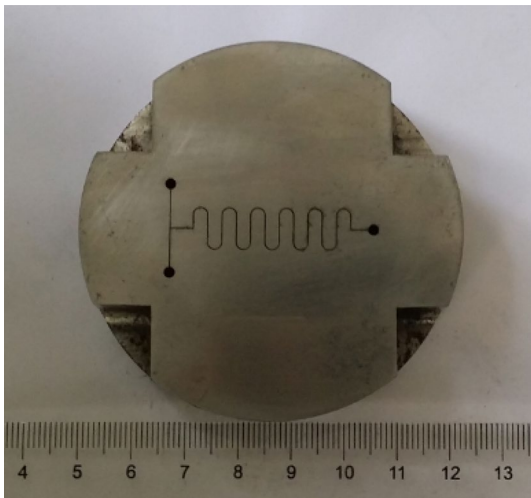


Fig. 6 Upper mold with a through-thickness microchannel

embossing. The lower platen is used for preheating and the upper one for embossing. The complete process contains mold preheating, embossing, holding, cooling and demolding. After that, the microchannel pattern is transferred to the PS film.

Experimental conditions are the same as those used in the simulation. Namely, the deformation of the PS film and SR pad is performed under varied embossing temperature from 90 to 110 °C, varied embossing load from 7.5 to 17.5 kN and varied Shore hardness of SR from 30 to 60 A. The effects of these key process parameters on the replication of the microchannel pattern were studied and compared experimental and numerically.

4 Results and discussion

In order to validate the proposed process model, simulation results were compared with experimental results obtained under various embossing conditions. The cross-sectional geometry (including channel depth and thickness) of the embossed PS films were measured and compared with those obtained from simulations. The film thickness varies with the position on the channel, and measurements were therefore taken at multiple points of the cross-section. In the following plots of channel thickness, the abscissa of the starting point corresponding to the center of the microchannel is set to 0 μm.

4.1 Channel depths predicted by simulations

Figure 7 shows predicted channel depths with different embossing temperatures, loads and hardness of silicone rubber. The depth of replication slightly reduces with the

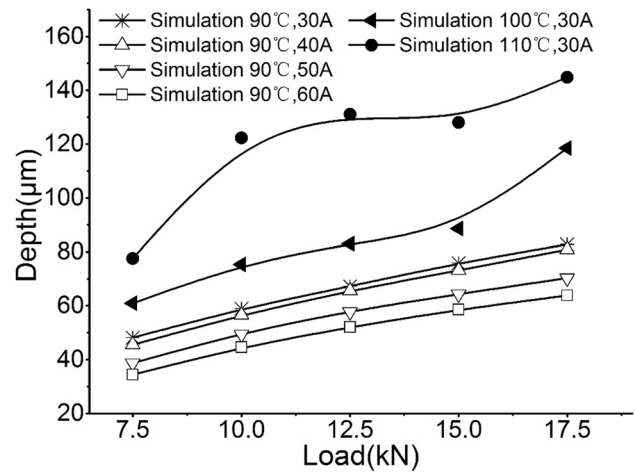


Fig. 7 Predicted channel depths at different embossing conditions

increase of the SR hardness. By comparison, the replication depth more significantly depends on the embossing temperature; it increases with increasing embossing temperature. Especially, the increase in replication depth is substantial when the embossing temperature changes from 100 to 110 °C. This is understandable since the PS film undergoes glass transition at 100 °C and above that temperature is rapidly converted into a rubbery material. In general, the embossing temperature is a predominating process parameter in rubber-assisted embossing since it determines the rheological properties of the embossing film. As expected, the effect of the embossing load is also significant; this effect arises from the relative hardness of the embossing film in a load-guided embossing process. These results agree well with the findings of Zhao et al. (2012).

4.2 Comparison between experiments and simulations

Figure 8a presents a comparison of replicated microchannel depths between simulations and experiments for different embossing conditions. It appears that predicted depths are in close proximity to experimental ones at the same conditions. The tendency is similar; the microchannel depth gradually increases with an increase of embossing temperature or embossing load. However, a relative large difference in replication depth (almost 20 μm) between simulation and experiment is observed at 17.5 kN load, 100 °C temperature and 50 A rubber hardness. Zhao et al. (2012) observed the storage modulus of PS experiences a broad transition around 100 °C and considered a transition temperature in the vicinity of 100 °C. The difference may be explained by the experimental microchannel depth of PS being derived from combined viscous and elastic deformation with the diminished storage modulus in the vicinity of the transition temperature.

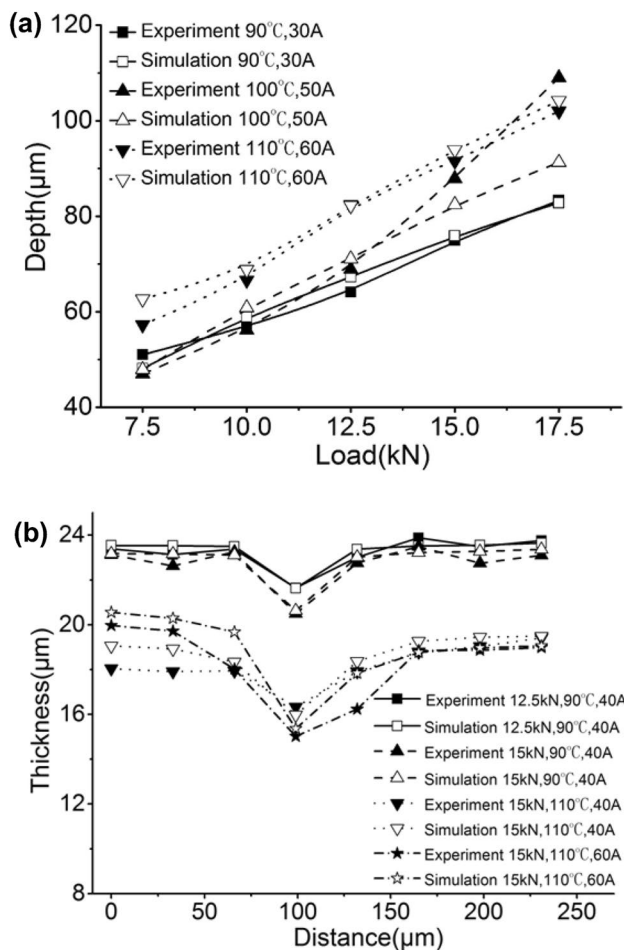


Fig. 8 Comparison of microchannel replication results between experiments and simulations at different embossing conditions: **a** channel depth curves; **b** thickness vs. distance curves

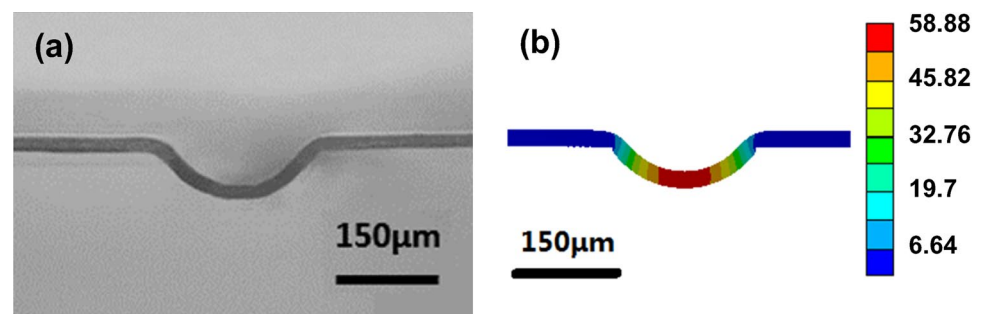
Figure 8b shows the thickness distributions between the experimental results and the simulation predictions at different SR hardness, temperature and load. In general, the predicted thickness distributions agree well with the experimental results. All thickness curves experience a distinct decrease at 100 μm owing to a stress contribution from the edge between mold and microchannel. The mean and variance of the thickness can be calculated and

used to quantify the comparison. At 12.5 kN load, 90 $^{\circ}\text{C}$ temperature and 40 A rubber hardness, the mean and variance of thickness from experiments are 23.25 μm and 0.349, respectively. Under the same embossing condition, the simulation results indicate that the mean thickness is 23.38 μm and the variance is 0.353. Analogously, at 15 kN, 90 $^{\circ}\text{C}$ and 40 A, the experimental mean and variance of microchannel thickness are 22.87 μm and 0.757, while the simulation results are 22.99 μm and 0.639. The experimental and simulation results, although fluctuating in a small range, also present a good agreement at 15 kN, 110 $^{\circ}\text{C}$ and 60 A. At this processing condition, slight differences emerge in microchannel thickness in which experimentally measured values are slightly less than those from the simulation. These results support that the hyperelastic process model is capable of predicting the general process characteristics of rubber-embossing with a through-thickness mold.

The primary reasons for the deviation between simulations and experiments are further explored as follows. Firstly, the simulation is performed under ideal isothermal conditions with a constant embossing load, and the effects of loading time and the variation of temperature including non-isothermal cooling that can be significant in an actual experiment are not considered. Secondly, the geometrical model and boundary conditions used in the process model are simplified. For example, the model is two-dimensional, and three-dimensional effects are not treated. SR is also unrealistically regarded as an incompressible rubber material. Nevertheless, the predictions are in general agreements with the experiments, especially for the thickness distribution. With further incorporation of a non-isothermal holding stage and more realistic material parameters and boundary conditions, the accuracy of the model can be improved.

Figure 9 showed the embossed shape of the PS film in which the thickness and the depth are quite similar between the simulation and the experiment at an embossing condition of 12.5 kN, 90 $^{\circ}\text{C}$ and 50 A. The flexible microchannel after sealing is shown in Fig. 10. The microchannel with the most uniform thickness and largest depth was predicted to occur at 20 kN, 90 $^{\circ}\text{C}$ and 30 A. This again agrees with the experimental findings.

Fig. 9 Deformed PS film at an embossing condition of 12.5 kN, 90 $^{\circ}\text{C}$ and 50 A: **a** from the experiment; **b** from the simulation



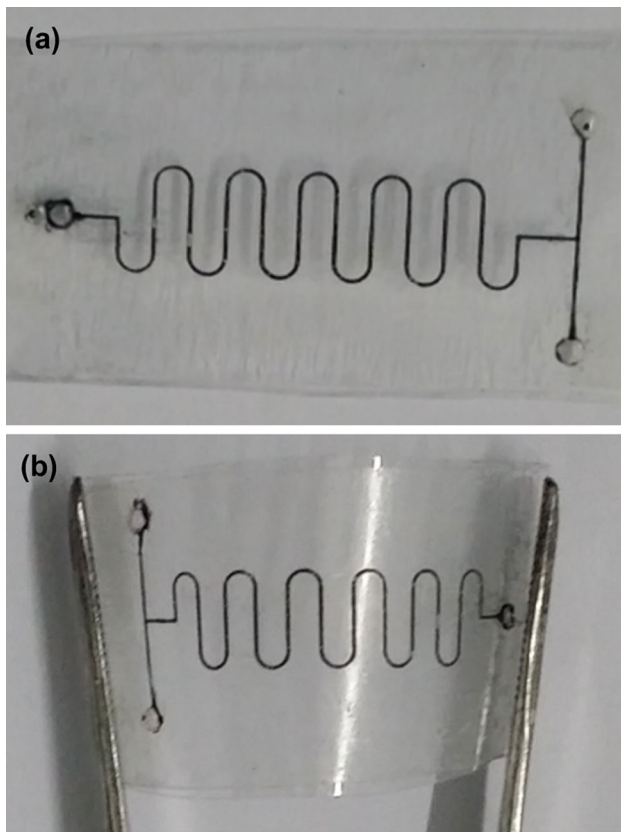


Fig. 10 Microchannels after sealing: **a** flat pattern; **b** bended pattern

5 Conclusions

Experimental and simulation studies of the film deformation process in rubber-assisted hot embossing with a through-thickness microchannel mold were conducted under uniform embossing conditions near the glass transition temperature. Firstly, microchannels were successfully replicated onto thin polystyrene films pressurized by a rubber pad as a soft counter-tool against a through-thickness microchannel hard mold. With this method, the mold design with otherwise a pair of hard contact mold plates is simplified, smoother surfaces on the embossed film is produced, and air in the mold cavity can be freely displaced to avoid the unwanted diesel effect. Secondly, the embossing temperature was found both in experiments and simulations to be the most influential process parameter affecting the replication quality of the microchannel, particularly the microchannel depth and the thickness distribution. Both experiments and simulations showed that an embossing temperature slightly above T_g is suitable for achieving a

uniform embossing thickness. The simulation results also agreed very well with the experimental observations for the effects of the embossing pressure and the rubber hardness on the replication quality. These results indicated that the process dynamics model using a hyperelastic constitutive model is capable of predicting the basic characteristics of the rubber-assisted embossing process with a through-channel embossing mold and the use of such a process model can significantly reduce the time in optimization of the tooling and process setup in rubber-assisted embossing.

Acknowledgments This work was supported by the National Natural Science Foundation of China (NSFC) under Grant Number 51275071 and the National Key Basic Research Development Program of China (973 Program) under Grant Number 2012CB025905.

References

- Beda T (2007) Modeling hyperelastic behavior of rubber: a novel invariant-based and a review of constitutive models. *J Polym Sci Part B Polym Phys* 45:1713–1732
- Guo Y, Liu G, Zhu X, Tian Y (2007) Analysis of the demolding forces during hot embossing. *Microsyst Technol* 13:411–415
- Lan S et al (2009) A parameter study on the micro hot-embossing process of glassy polymer for pattern replication. *Microelectron Eng* 86:2369–2374
- Nagarajan P, Yao D (2006) Rubber-assisted hot embossing for structuring thin film polymeric films. 2006 ASME International Mechanical Engineering Congress and Exposition, Chicago
- Nagarajan P, Yao D (2009) Rubber-assisted micro forming of polymer thin films. *Microsyst Technol* 15:251–257
- Nagarajan P, Yao D (2011a) Uniform shell patterning using rubber-assisted hot embossing process. I. Experimental. *Polym Eng Sci* 51:592–600
- Nagarajan P, Yao D (2011b) Uniform shell patterning using rubber-assisted hot embossing process. II. Process analysis. *Polym Eng Sci* 51:601–608
- Park JM, Kang TG, Park SJ (2011) Numerical simulation of hot embossing filling stage using a viscoelastic constitutive model. *Korea Aust Rheol J* 23:139–146
- Song X, Shan XC, Chow SL, Deng XY, Teo WS (2015) Numerical and experimental study of the filling stage of roll-to-roll UV embossing process with micro features. *Microsyst Technol* 21:1729–1738
- Srivastava V, Chester SA, Ames NM, Anand L (2010) A thermo-mechanically-coupled large-deformation theory for amorphous polymers in a temperature range which spans their glass transition. *Int J Plast* 26:1138–1182
- Taylor H, Lam YC, Boning D (2009) A computationally simple method for simulating the micro-embossing of thermoplastic layers. *J Micromech Microeng* 19:75007
- Worgull M, Hecke M (2004) New aspects of simulation in hot embossing. *Microsyst Technol* 10:432–437
- Zhao D, Wyatt T, Wang M, Yi A, Yao D (2012) Rubber-assisted embossing of polymer thin films using molds with through-thickness microchannels. *Microsyst Technol* 18:481–488